



## OPEN ACCESS

## EDITED BY

Hai-Ying Wang,  
Nanjing Xiaozhuang University, China

## REVIEWED BY

Zi-Yi Du,  
Jiangxi Normal University, China  
Ke-zhao Du,  
Fujian Normal University, China

## \*CORRESPONDENCE

Jian-Rong Li,  
jrli@fjirsm.ac.cn  
Heng-Yun Ye,  
hyye@seu.edu.cn

## SPECIALTY SECTION

This article was submitted to Inorganic Chemistry, a section of the journal Frontiers in Chemistry

RECEIVED 14 June 2022

ACCEPTED 30 June 2022

PUBLISHED 05 August 2022

## CITATION

Wang Z-J, Li L-H, Feng Y, Wang Q-W, Wu L-K, Li J-R and Ye H-Y (2022), Synthesis, dielectric, magnetic, and photoluminescence properties of two new hybrid rare-earth double perovskites. *Front. Chem.* 10:969156. doi: 10.3389/fchem.2022.969156

## COPYRIGHT

© 2022 Wang, Li, Feng, Wang, Wu, Li and Ye. This is an open-access article distributed under the terms of the [Creative Commons Attribution License \(CC BY\)](https://creativecommons.org/licenses/by/4.0/). The use, distribution or reproduction in other forums is permitted, provided the original author(s) and the copyright owner(s) are credited and that the original publication in this journal is cited, in accordance with accepted academic practice. No use, distribution or reproduction is permitted which does not comply with these terms.

# Synthesis, dielectric, magnetic, and photoluminescence properties of two new hybrid rare-earth double perovskites

Ze-Jie Wang, Long-He Li, Yan Feng, Qin-Wen Wang, Ling-Kun Wu, Jian-Rong Li\* and Heng-Yun Ye\*

Chaotic Matter Science Research Center, Jiangxi University of Science and Technology, Ganzhou, China

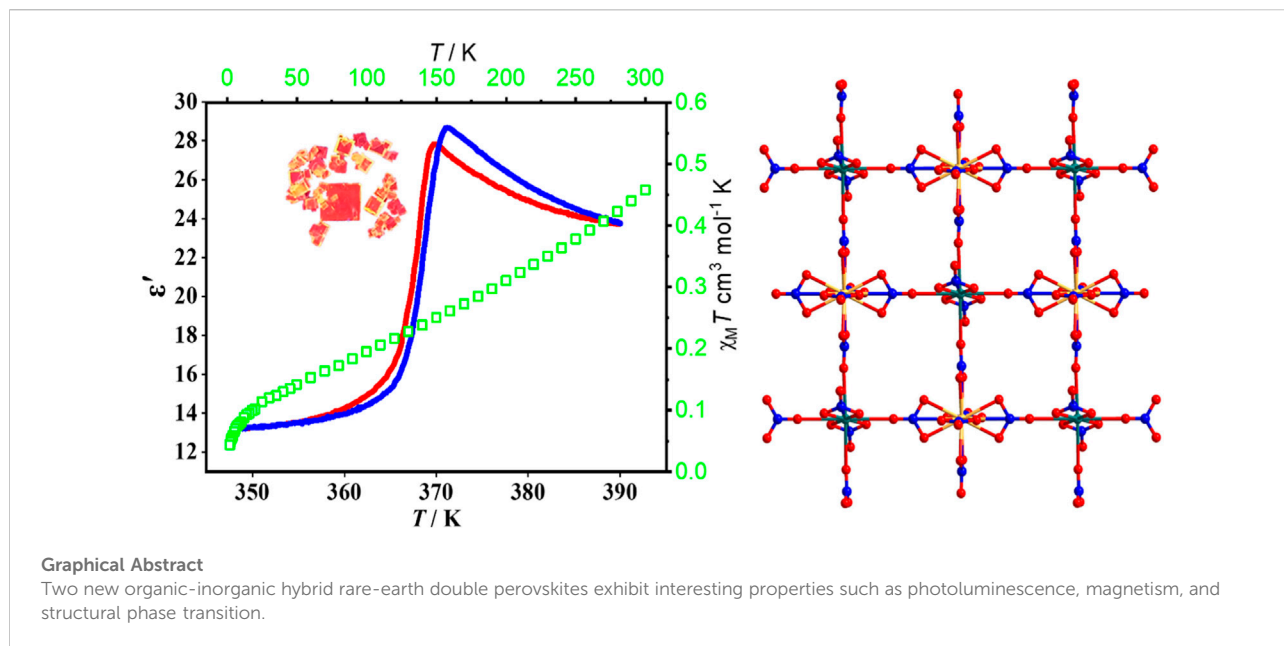
Two new organic–inorganic hybrid double perovskites  $(R3HQ)_4CsSm(NO_3)_8$  (**1**) ( $R3HQ = (R)-(-)-3$ -quinuclidinol) and  $(R3HQ)_4CsEu(NO_3)_8$  (**2**) were synthesized and characterized. Compounds **1** and **2** exhibit obvious phase transitions at 379 and 375 K, respectively, confirmed by differential scanning calorimetry (DSC) and variable temperature powder X-ray diffraction. The rapid switching between high- and low-dielectric states makes it a typical dielectric material with a switchable dielectric constant for thermal stimulus response. Furthermore, **1** and **2** show attractive photoluminescence and paramagnetic behavior, and the fluorescence quantum yield of **2** reached 14.6%. These results show that compounds **1** and **2** can be used as excellent candidates for multifunctional intelligent materials, which also provides a new way for development of multifunctional materials.

## KEYWORDS

organic–inorganic hybrid, rare earths, double perovskites, fluorescence, magnetic

## Introduction

Perovskite structure, typically of  $ABX_3$ -type perovskites, comprises a three-dimensional (3D) network by corner-sharing  $BX_6$  octahedra, where the B atom is a metal cation and the A-site cation is located in the octahedra center (Wang et al., 2021; Zhou et al., 2021; Xu et al., 2022). For ~20 years, extensive interest has been focused on organic–inorganic hybrid perovskites (OIHPs) owing to their potential applications in areas such as ferroelectric, piezoelectric, and photovoltaic, etc. (Saparov and Mitzi, 2016; Chen et al., 2019; Shi et al., 2020a; Zhou et al., 2021). Compared with pure inorganic perovskites, OIHPs show much flexible structural tunability due to the introduction of organic materials (Wang et al., 2021; Shao et al., 2022). More organic cations can be used as an ideal substitute for site A when the dimension of OIHPs is reduced from 3D to 2D due to the larger tolerance factor of the 2D compound (Li et al., 2019; Yang et al., 2019; Shi et al., 2020a; Zhang et al., 2020).



In principle, replacing the B site with two different metals will produce a double perovskite structure; this kind of double perovskite-like compound can provide higher structural variability and richer physical-chemical connotations, leaving great opportunities for multifunctional materials (Shi et al., 2020a; Ma et al., 2021). Much research interest focuses on exploring molecular-based multifunctional materials (Mao et al., 2019; Zhang et al., 2021). The versatility of the material depends on the coordination of the metal (Pan et al., 2000; Zhang et al., 2013; Som et al., 2014; Kim et al., 2015; Huang et al., 2017; Li B. et al., 2018; Chen et al., 2019; Xue et al., 2020), for example, rare-earth ions have rich coordination modes and unique photoluminescence and magnetic properties because of the characteristics of their electronic configuration. They are used as one of the metals to assemble double perovskites to easily form multifunctional materials, which makes them a good candidate for the construction of multifunctional bimetallic perovskite materials (Zhang et al., 2021).

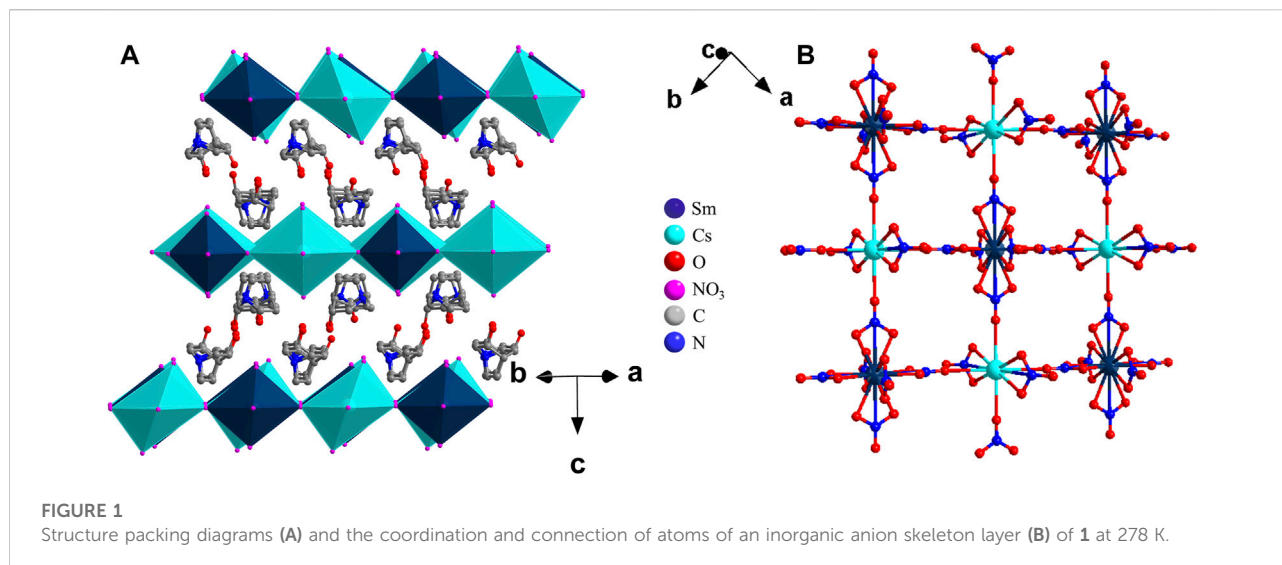
Compared with organic-inorganic hybrid halide perovskites developed rapidly with halogen atoms as the bridging ligand, there are few reports on the synthesis of double perovskite structure compounds using multi-atom nitrate as the bridging ligand (Xu et al., 2016). In 2020, we reported on a family of rare-earth double perovskite compounds, in which ferroelectric, piezoelectric, and fluorescent properties were successfully achieved (Shi et al., 2020a; Shi et al., 2020b; Hua et al., 2020). Inspired by these works, two new rare-earth alkali metal double perovskite-type compounds were synthesized by introducing rare-earth ions into the B site of double perovskite and using  $\text{NO}_3^-$  as the bridging ligand:  $(\text{R3HQ})_4\text{CsSm}(\text{NO}_3)_8$  (**1**) and  $(\text{R3HQ})_4\text{CsEu}(\text{NO}_3)_8$  (**2**) (R3HQ = (R)-(-)-3-quinuclidinol).

The compounds not only undergo a reversible structural phase transition at about 379 K for **1** and 375 K for **2** but the phase temperature is also increased by about 30 K compared to the reported  $(\text{R3HQ})_4\text{RbSm}(\text{NO}_3)_8$  and  $(\text{R3HQ})_4\text{RbSm}(\text{NO}_3)_8$ . Interestingly, **1** and **2** exhibit photoluminescence under UV excitation, and the quantum yield of **2** reached 14.6%. In addition, the direct current (DC) magnetic susceptibility of compounds shows obvious paramagnetic signals. The successful construction of the compounds provides a new idea for further enriching the rare-earth double perovskite system (Zhang et al., 2020). The fast switchable dielectric behaviors, and photoluminescence and magnetic properties make them an ideal candidate for multifunctional materials (Rok et al., 2019).

## Experimental

### Synthesis of $(\text{R3HQ})_4\text{CsSm}(\text{NO}_3)_8$ (**1**) and $(\text{R3HQ})_4\text{CsEu}(\text{NO}_3)_8$ (**2**)

All reagents were purchased commercially and used as received without any further purification. First, an unseparated R3HQNO<sub>3</sub> (R3HQ = (R)-(-)-3-quinuclidinol) aqueous solution was obtained by adding R3HQ and HNO<sub>3</sub> solution (65–68%) to an aqueous solution in a molar ratio of 1:1. Then, high-quality colorless transparent block crystals were obtained by slowly evaporating the mixed aqueous solution of  $\text{Sm}(\text{NO}_3)_3/\text{Eu}(\text{NO}_3)_3$ ,  $\text{CsNO}_3$ , and R3HQNO<sub>3</sub> in a molar ratio of 1:1:2 at room temperature for about 2 weeks. Anal. (%) Calc. for  $\text{C}_{28}\text{H}_{56}\text{CsSmN}_{12}\text{O}_{28}$ : C, 25.25, H, 4.23, N, 13.94. Found: C, 26.03,



H, 4.37, N, 13.01. Anal. (%) Calc. for  $C_{28}H_{56}CsEuN_{12}O_{28}$ : C, 25.30, H, 4.19, N, 13.17. Found: C, 26.00, H, 4.36, N, 12.99.

## General measurements

DSC measurements were performed with a NETZSCH differential scanning calorimeter 214 Polyma in the temperature range 300–390 K under atmospheric pressure with a 20 K  $\text{min}^{-1}$  heating/cooling rate by heating and cooling the crystalline samples. The real part  $\epsilon'$  of the complex permittivity which is related to the temperature was performed using a TH2828A variable temperature dielectric measuring instrument in the temperature range of about 345–390 K. The variable temperature powder X-ray diffraction data were measured on a Rigaku D/MAX 2000 PC X-ray diffraction system with  $\text{Cu-K}\alpha$  radiation in the  $2\theta$  range of  $5^\circ$ – $50^\circ$  with a step size of  $0.02^\circ$  and in the temperature range 298–403 K. Photoluminescence was recorded on an Edinburgh FL980 UV/V/NIR fluorescence spectrometer. The quantum yield was measured by using an Edinburgh FLS 1000 UV/V/NIR fluorescence spectrometer. The single-crystal X-ray diffraction data were collected on a Rigaku Synergy apparatus with graphite-monochromate  $\text{Mo-K}\alpha$  radiation at 278 K for **1** and 301 K for **2**, respectively. Thermogravimetric analysis was performed on NETZSCH STA 449F3 in the temperature range of about 298–1070 K.

## Results and discussion

### Crystal structure

Single crystal X-ray diffraction studies revealed that **1** crystallized in the tetragonal chiral space group  $P4_322$  (no. 95)

at 278 K with cell parameter  $a = 10.1274(1) \text{ \AA}$ ,  $b = 10.1274(1) \text{ \AA}$ ,  $c = 46.2252(11) \text{ \AA}$ , and  $Z = 4$ . The crystallographic asymmetric unit of **1** comprises Sm and Cs sharing a nitrate and each connecting a complete nitrate and an incomplete nitrate, and two separate organic cations, the complete molecules being generated by inversion symmetry. Both Sm and Cs are coordinated with six  $\text{NO}_3^-$  as bridging ligands to chelate into an alternately arranged corner-sharing octahedral structure to form a framework of inorganic metal layers, and the double layer of R3HQ organic cations occupied the space between the inorganic layers (Figure 1). The distance between the two adjacent inorganic metal layers is about 11.56  $\text{ \AA}$ , where the distance between Sm–Sm or Cs–Cs and Sm–Cs is about 12.78  $\text{ \AA}$  and 12.62  $\text{ \AA}$ , respectively. The distance between Sm–Cs in the same inorganic metal layer is 7.16  $\text{ \AA}$ . Therefore, the resulting octahedron is slightly distorted rather than the standard regular octahedron. The organic cation layer and inorganic metal framework layer are interleaved along the  $c$ -axis, and there are four inorganic layers in one cell. All C–O bonds in the organic layer are arranged along the  $c$ -axis, therefore, forming an infinite octahedron corner-sharing  $A_4B^{\text{III}}X_8$ -type two-dimensional layered organic–inorganic hybrid double-metal perovskite structure. The structure of **2** is similar to that of **1** and is not described in detail here (Supplementary Figure S1).

We first carried out powder X-ray diffraction (PXRD) of **1** and **2** at 298 K (Supplementary Figure S2). It can be seen that the as-synthesized samples are a single pure phase, and all subsequent analyses and measurements are based on this premise. Preliminary thermal analysis has shown that the two compounds undergo a reversible structural phase transition. To further reveal the cause of the phase transition of these compounds, variable temperature X-ray single-crystal

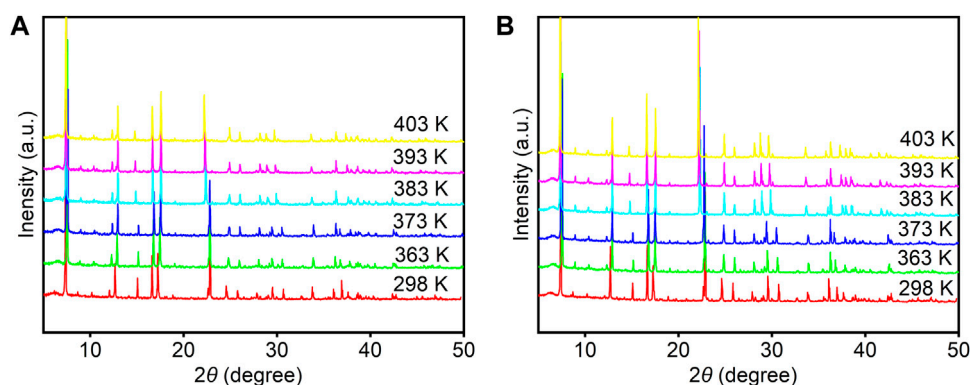


**FIGURE 2**  
Variable temperature PXRD patterns of **1** (A) and **2** (B).

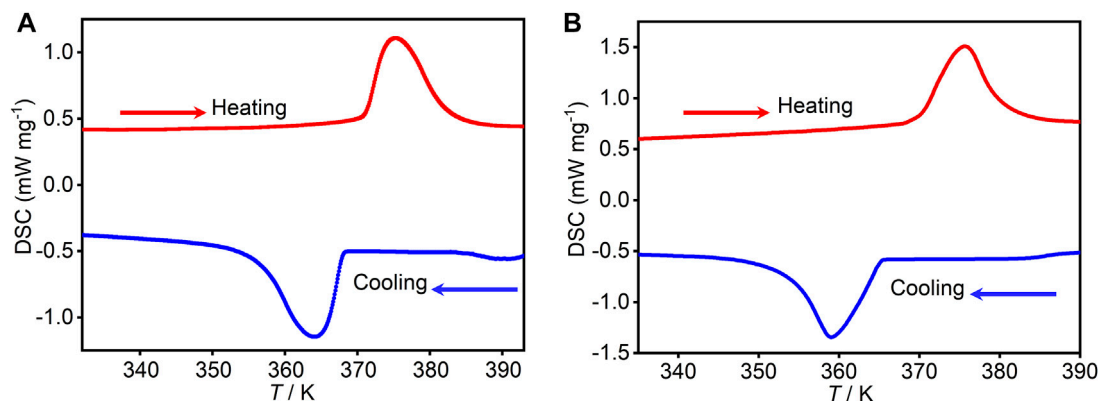


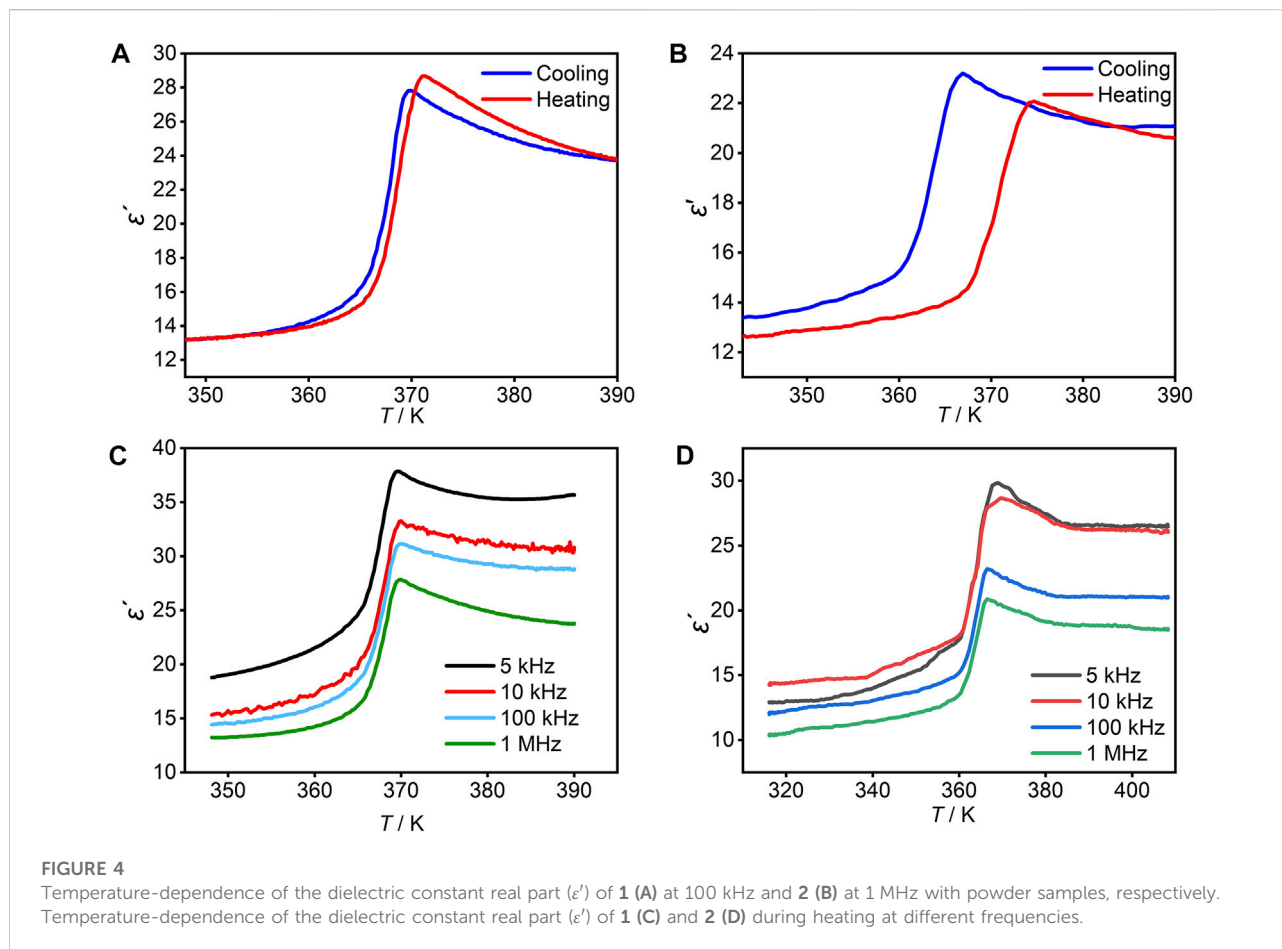
**FIGURE 3**  
DSC curves of **1** (A) and **2** (B) measured under nitrogen and atmospheric pressure at a heating/cooling rate of 20 K min<sup>-1</sup> at a temperature range of 330–400 K.

diffraction was carried out. When the temperature was above the phase transition temperature, we were unable to obtain X-ray single-crystal diffraction data because of their poor crystal quality. It is speculated that the crystal structure changes dramatically, which is caused by the excessive latent heat during the phase transition (Tang Y.-Z. et al., 2015; Ye et al., 2016; Harada et al., 2018; Yang et al., 2019; Xu et al., 2021). Therefore, variable temperature PXRD measurements were performed to determine whether the structures of **1** and **2** changed as the temperature increased. The PXRD patterns of **1** and **2** (Figures 2A,B, Supplementary Figure S3) remain unchanged in the temperature range from 298–373 K. However, the diffraction peak of the PXRD patterns appear to change including shift, disappear, increase, and even the distance

between part diffraction peaks changes obviously when the temperature continues to rise 383 K above the phase transition temperature, indicating that the crystal structure has changed because of the temperature change. The results are consistent with DSC and dielectric behavior analysis.

## Phase transition

Differential scanning calorimetry (DSC) is an effective thermodynamic method used for determining whether crystals undergo phase transition resulting from temperature induction. The phase transitions of **1** and **2** were investigated by DSC under nitrogen and atmospheric pressure with a heating/cooling rate of



20 K  $\text{min}^{-1}$ . The DSC curve (Figure 3A) of **1** displays an obvious thermal anomaly peak at 379 K upon heating, and the corresponding thermal anomaly peak appeared at 358 K upon cooling. Compared with the reported  $(\text{R3HQ})_4\text{RbSm}(\text{NO}_3)_8$  and  $(\text{R3HQ})_4\text{RbSm}(\text{NO}_3)_8$ , the phase transition temperature is increased by about 30 K. Its average temperature is taken and calculated, and the change in entropy and enthalpy is 17.44 kJ  $\text{mol}^{-1}$  and 46.0254 J  $\text{mol}^{-1} \text{K}^{-1}$ , respectively. Similarly, compound **2** showed corresponding thermal anomaly peaks at 375 and 359 K (Figure 3B). The change in entropy and enthalpy is 21.02 kJ  $\text{mol}^{-1}$  and 56.0608 J  $\text{mol}^{-1} \text{K}^{-1}$ , respectively. That is, the change of rare-earth elements in adjacent positions has little thermal change for compounds with the same configuration. According to the Boltzmann equation,  $\Delta S = R \ln(N)$ , where  $R$  is the gas constant and  $N$  is the ration of the number of respective geometrically distinguishable orientations in high- and low-temperature phases (Zhao et al., 2019), the values of  $N_1$  and  $N_2$  are calculated as 1.0043 and 1.0052, respectively. The small  $N$  values indicated the complex phase transition mechanism (Fu et al., 2012; Sun et al., 2012; Tang Y. et al., 2015; Sun et al., 2015; Li S.-G. et al., 2018). Combining the obvious thermal hysteresis of about 21 and 16 K during the heating–cooling cycles and wide

peak patterns revealed obvious first-order phase transition characteristics. Moreover, according to the thermogravimetric (TG) curves, the phase transition temperature was significantly lower than its decomposition temperature of **1** and **2** (Supplementary Figure S4), which also confirmed that the phase transition was not caused by the decomposition of compounds.

## Dielectric properties

The dielectric constant is the most basic parameter to measure dielectric materials (Fu et al., 2008a; Fu et al., 2008b; c). The real part ( $\epsilon'$ ) of the temperature-dependent dielectric constant of **1** was investigated in the temperature range of 348–390 K and the frequency of 100 kHz. The dielectric constant shows a trend of slow increase in the range of about 348–365 K, and a trend of slow decrease in the temperature range of about 369–395 K (Figure 4A). However, the dielectric constant changes sharply by about 2-fold in these two temperature ranges. An obvious “step-like” anomaly appeared at 371 K upon the heating process, and the corresponding anomaly appeared at 369.7 K upon the cooling

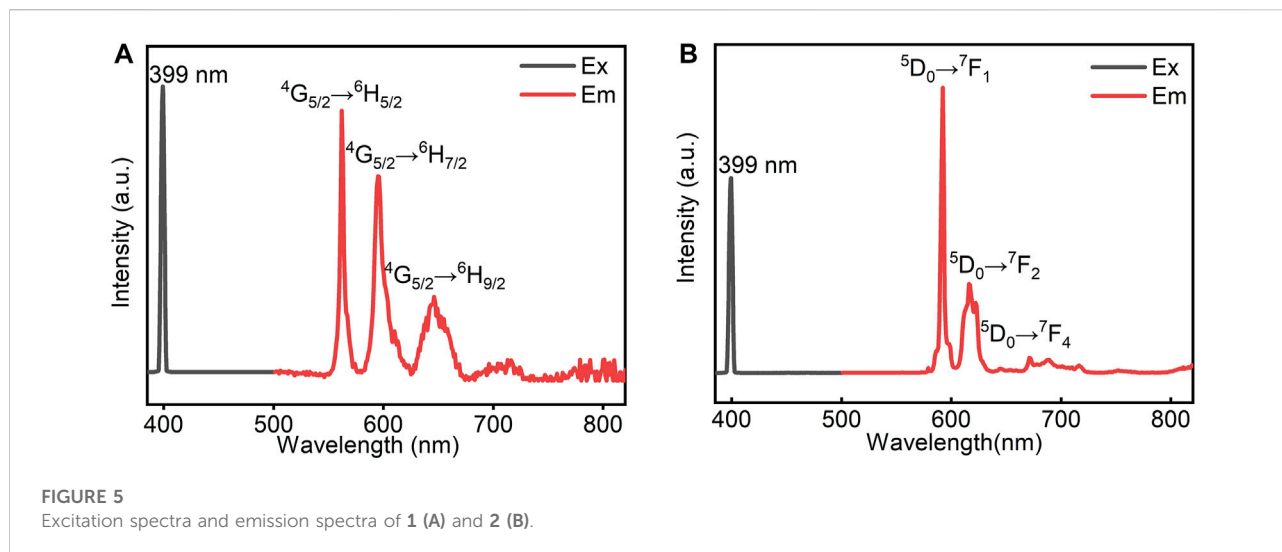


FIGURE 5  
Excitation spectra and emission spectra of **1** (A) and **2** (B).

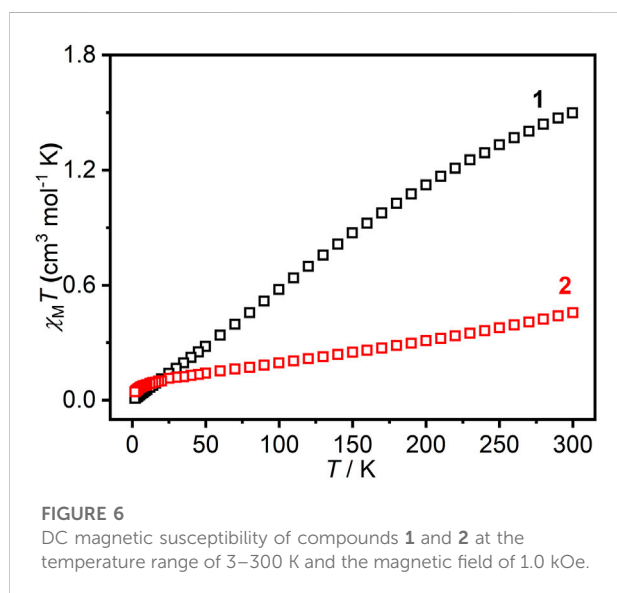


FIGURE 6  
DC magnetic susceptibility of compounds **1** and **2** at the temperature range of 3–300 K and the magnetic field of 1.0 kOe.

process. Similarly, it can be seen that in the temperature range of 345–395 K and the frequency of 1 MHz, the real part of the dielectric constant of **2** also shows a trend of slow increase first, then a sharp rise by about 2-fold, and finally, slow decline (Figure 4B). In the heating process, there is an obvious “step-like” abnormality at 374.7 K, and corresponding steps appear at 366.8 K in the cooling process. Reversible dielectric anomalies during the heating–cooling cycle confirm the reversible phase transition of the compounds. That is, the real part of the dielectric constant of the compounds can be adjusted between the high and low dielectric states, indicating that the compounds are a good candidate for switching dielectric materials in response to thermal stimuli. This reversible transition between high and low dielectric states confirms DSC measurements that the compounds undergo a first-order reversible phase transition. In

addition, it can be seen that the permittivity of the compounds varies with frequency at the same temperature, with an obvious frequency dependence (Figure 4C, Figure 4D). This is due to the effect of the external electric field, and the polarization of the dielectric cannot keep up with the change in the alternating electric field when the frequency increases, which causes dielectric loss (Gridnev and Trukhachev, 2013; Khanchaitit et al., 2013).

## Photoluminescence properties

One of the purposes of introducing rare-earth ions to construct a double metal perovskite structure is to combine the photoluminescence properties of rare-earth ions. Photoluminescence is caused by electron transitions of unpaired 4f electrons. In particular, **2** showed a distinct orange light visible to the naked eye under UV light. As shown in Figure 5A, there are three strong absorption peaks at 562, 596, and 646 nm in the emission spectrum of **1**, which are caused by the  ${}^4G_{5/2} \rightarrow {}^6H_{5/2}$ ,  ${}^4G_{5/2} \rightarrow {}^6H_{7/2}$ , and  ${}^4G_{5/2} \rightarrow {}^6H_{9/2}$  transitions of  $\text{Sm}^{\text{III}}$ , respectively. Similarly, three strong absorption peaks and one weak absorption were observed at 592, 616, and 671 nm in the emission spectrum of **2** (Figure 5B), which were caused by the  ${}^5D_0 \rightarrow {}^7F_1$ ,  ${}^5D_0 \rightarrow {}^7F_2$ , and the relatively weak  ${}^5D_0 \rightarrow {}^7F_4$  transitions of  $\text{Eu}^{\text{III}}$ , respectively. Among them, the magnetic dipole transition  ${}^5D_0 \rightarrow {}^7F_1$  is obviously stronger than the electric dipole transition  ${}^5D_0 \rightarrow {}^7F_2$  because  $\text{Eu}^{\text{III}}$  is in an almost centrally symmetric position. The fluorescence quantum yield of **2** reached 14.6%. The solid-state optical absorption spectra of **1** and **2** were measured by the diffuse reflectance technique (Supplementary Figure S5). The band gaps, estimated from the absorption edges, are 3.71 eV for **1** and 3.81 eV for **2**, which are in agreement with their crystal colors.

## Magnetic properties

The direct current (DC) magnetic susceptibility of compounds **1** and **2** was measured in the temperature range of 2–300 K under 1.0 kOe with powder samples (Figure 6). In general, the value of  $\chi_m T$  is zero for  $\text{Eu}^{\text{III}}$  due to  $J = 0$ , but an obvious paramagnetic signal was observed from the experimental data. This is because the first excited state of  $\text{Eu}^{\text{III}}$  is too close to the ground state ( $300 \text{ cm}^{-1}$ ), which leads to the population of excited states. The ground state energy level is split into seven  ${}^7F_1$  states caused by spin-orbit coupling. Hence,  $J$  is no longer 0, it can change from 0 to 6. Therefore, the value of  $\chi_m T$  gradually decreases and approaches 0 with the decrease in temperature. For **2**,  $\text{Sm}^{\text{III}}$  is the same as  $\text{Eu}^{\text{III}}$ , the value of  $\chi_m T$  decreases gradually with the decrease in temperature, which is a paramagnetic signal.

## Conclusion

In summary, we obtained two organic–inorganic hybrid rare-earth double perovskites, which adopt a Ruddlesden–Popper (RP)-type perovskite structure. The reversible dielectric phase transition and switchable dielectric constant between high- and low-dielectric states of the compounds are verified by measuring temperature-dependence of the real part of the dielectric constant using differential scanning calorimetry (DSC) and variable temperature PXRD. Simultaneously, the compounds also have significant photoluminescence and paramagnetic behavior. Therefore, the compounds have potential application in the field of stimulus-responsive multifunctional intelligent materials, and the successful synthesis of the two compounds further enriches the rare-earth two-dimensional perovskite family.

## Data availability statement

The raw data supporting the conclusion of this article will be made available by the authors, without undue reservation.

## References

- Chen, X., Xu, J., Xu, Y., Luo, F., and Du, Y. (2019). Rare Earth double perovskites: a fertile soil in the field of perovskite oxides. *Inorg. Chem. Front.* 6 (9), 2226–2238. doi:10.1039/c9qi00512a
- Fu, D.-W., Ye, H.-Y., Ye, Q., Pan, K.-J., and Xiong, R.-G. (2008a). Ferroelectric metal-organic coordination polymer with a high dielectric constant. *Dalton Trans.* (7), 874–877. doi:10.1039/b714293e
- Fu, D.-W., Zhang, W., and Xiong, R.-G. (2008b). The first metal-organic framework (MOF) of Imazethapyr and its SHG, piezoelectric and ferroelectric properties. *Dalton Trans.* (30), 3946–3948. doi:10.1039/b806255b

## Author contributions

Z-JW: methodology, validation, data curation, formal analysis, investigation, and writing—original draft. L-HL: magnetic testing and data analysis. YF: conceptualization, data curation, and visualization. Q-WW: conceptualization and methodology. L-KW: visualization and data curation. J-RL: writing—original draft, formal analysis, investigation, data curation, visualization, writing—review and editing, and funding acquisition. H-YY: resources, writing—review and editing, supervision, and project administration.

## Funding

This work was supported by the National Natural Science Foundation of China (21875093) and Natural Science Foundation of Jiangxi Province (20204BCJ22015 and 20202ACBL203001).

## Conflict of interest

The authors declare that the research was conducted in the absence of any commercial or financial relationships that could be construed as a potential conflict of interest.

## Publisher's note

All claims expressed in this article are solely those of the authors and do not necessarily represent those of their affiliated organizations, or those of the publisher, the editors, and the reviewers. Any product that may be evaluated in this article, or claim that may be made by its manufacturer, is not guaranteed or endorsed by the publisher.

## Supplementary material

The Supplementary Material for this article can be found online at: <https://www.frontiersin.org/articles/10.3389/fchem.2022.969156/full#supplementary-material>

- Fu, D.-W., Zhang, W., and Xiong, R.-G. (2008c). Isotope effect on SHG response and ferroelectric properties of a homochiral zinc coordination compound containing tetrazole ligand. *Cryst. Growth Des.* 8 (9), 3461–3464. doi:10.1021/cg800507k

- Fu, D.-W., Zhang, Y., Cai, H.-L., Zhu, H.-m., Chen, X.-y., Xiong, R.-G., et al. (2012). The first example of a molecule-based ferroelectric with barium cation: Catena-( $\mu_2$ -nitrito-O, O)-bi-aqua-(18-crown-6)-barium nitrite. *J. Mater. Chem.* 22 (34), 17525. doi:10.1039/c2jm32662k

- Gridnev, S. A., and Trukhachev, S. E. (2013). The dielectric loss mechanism at the phase transition in improper ferroelectric crystal of

- terbium molybdate. *Ferroelectrics* 443 (1), 63–67. doi:10.1080/00150193.2012.747398
- Harada, J., Yoneyama, N., Yokokura, S., Takahashi, Y., Miura, A., Kitamura, N., et al. (2018). Ferroelectricity and piezoelectricity in free-standing polycrystalline films of plastic crystals. *J. Am. Chem. Soc.* 140 (1), 346–354. doi:10.1021/jacs.7b10539
- Hua, M.-M., Ye, L., Wang, Q.-W., Ma, J.-J., Gong, Z.-X., Xu, Q., et al. (2020). A layered hybrid rare-Earth double-perovskite-type molecule-based compound with electrical and optical response properties. *J. Mater. Chem. C* 8 (46), 16349–16353. doi:10.1039/d0tc04386a
- Huang, X. Y., Li, B., Guo, H., and Chen, D. Q. (2017). Molybdenum-doping-induced photoluminescence enhancement in  $\text{Eu}^{3+}$ -activated  $\text{CaWO}_4$  red-emitting phosphors for white light-emitting diodes. *Dyes Pigm.* 143, 86–94. doi:10.1016/j.dyepig.2017.04.037
- Khanchaitit, P., Han, K., Gadinski, M. R., Li, Q., and Wang, Q. (2013). Ferroelectric polymer networks with high energy density and improved discharged efficiency for dielectric energy storage. *Nat. Commun.* 4, 2845. doi:10.1038/ncomms3845
- Kim, M. K., Moon, J. Y., Choi, H. Y., Oh, S. H., Lee, N., Choi, Y. J., et al. (2015). Investigation of the magnetic properties in double perovskite  $\text{R}_2\text{CoMnO}_6$  single crystals (R = rare Earth: La to Lu). *J. Phys. Condens. Matter* 27 (42), 426002. doi:10.1088/0953-8984/27/42/426002
- Li, B., Huang, X. Y., Guo, H., and Zeng, Y. J. (2018). Energy transfer and tunable photoluminescence of  $\text{LaBWO}_6$ :  $\text{Tb}^{3+}$ ,  $\text{Eu}^{3+}$  phosphors for near-UV white LEDs. *Dyes Pigm.* 150, 67–72. doi:10.1016/j.dyepig.2017.11.003
- Li, L., Liu, X., Li, Y., Xu, Z., Wu, Z., Han, S., et al. (2019). Two-dimensional hybrid perovskite-type ferroelectric for highly polarization-sensitive shortwave photodetection. *J. Am. Chem. Soc.* 141 (6), 2623–2629. doi:10.1021/jacs.8b12948
- Li, S.-G., Li, T.-t., Liu, R.-T., and Xiong, X. (2018). Synthesis, crystal structure, and hydrogen-bonded displacive-type structural phase transition of guanidine dichloroacetate. *Struct. Chem.* 29 (2), 451–456. doi:10.1007/s11224-017-1042-8
- Ma, J.-J., Xu, Q., Wang, Q.-W., Gong, Z.-X., Shi, C., Ye, H.-Y., et al. (2021). Structure phase transition and dielectric switching in an organic-inorganic hybrid rare-Earth double perovskite-type compound:  $(\text{DMP})_2\text{LaRb}(\text{NO}_3)_6$  (DMP = N, N-dimethylpyrrolidinium cation). *J. Rare Earths* 40, 937–941. doi:10.1016/j.jre.2021.05.010
- Mao, L., Stoumpos, C. C., and Kanatzidis, M. G. (2019). Two-dimensional hybrid halide perovskites: Principles and promises. *J. Am. Chem. Soc.* 141 (3), 1171–1190. doi:10.1021/jacs.8b10851
- Pan, L., Huang, X. Y., Li, J., Wu, Y. G., and Zheng, N. W. (2000). Novel single- and double-layer and three-dimensional structures of rare-Earth metal coordination polymers: The effect of lanthanide contraction and acidity control in crystal structure formation. *Angew. Chem. Int. Ed.* 39 (3), 527–530. doi:10.1002/(sici)1521-3773(20000204)39:3<527::aid-anie527>3.0.co;2-w
- Rok, M., Moskwa, M., Dzialowa, M., Bienko, A., Rajnak, C., Boca, R., et al. (2019). Multifunctional materials based on the double-perovskite organic-inorganic hybrid  $(\text{CH}_3\text{NH}_3)_2\text{KCr}(\text{CN})_6$  showing switchable dielectric, magnetic, and semiconducting behaviour. *Dalton Trans.* 48 (44), 16650–16660. doi:10.1039/c9dt03553b
- Saparov, B., and Mitzi, D. B. (2016). Organic-inorganic perovskites: Structural versatility for functional materials design. *Chem. Rev.* 116 (7), 4558–4596. doi:10.1021/acs.chemrev.5b00715
- Shao, T., Ren, R. Y., Huang, P. Z., Ni, H. F., Su, C. Y., Fu, D. W., et al. (2022). Metal ion modulation triggers dielectric double switching and green fluorescence in  $\text{A}_2\text{MX}_4$ -type compounds. *Dalton Trans.* 51 (5), 2005–2011. doi:10.1039/d1dt03948b
- Shi, C., Ye, L., Gong, Z.-X., Ma, J.-J., Wang, Q.-W., Jiang, J.-Y., et al. (2020a). Two-dimensional organic-inorganic hybrid rare-earth double perovskite ferroelectrics. *J. Am. Chem. Soc.* 142 (1), 545–551. doi:10.1021/jacs.9b11697
- Shi, C., Ma, J.-J., Jiang, J.-Y., Hua, M.-M., Xu, Q., Yu, H., et al. (2020b). Large piezoelectric response in hybrid rare-earth double perovskite relaxor ferroelectrics. *J. Am. Chem. Soc.* 142 (21), 9634–9641. doi:10.1021/jacs.0c00480
- Som, S., Kunti, A. K., Kumar, V., Kumar, V., Dutta, S., Chowdhury, M., et al. (2014). Defect correlated fluorescent quenching and electron phonon coupling in the spectral transition of  $\text{Eu}^{3+}$  in  $\text{CaTiO}_3$  for red emission in display application. *J. Appl. Phys.* 115 (19), 193101. doi:10.1063/1.4876316
- Sun, Z., Chen, T., Luo, J., and Hong, M. (2012). Bis(imidazolium) L-tartrate: a hydrogen-bonded displacive-type molecular ferroelectric material. *Angew. Chem. Int. Ed.* 51 (16), 3871–3876. doi:10.1002/anie.201200407
- Sun, Z., Tang, Y., Zhang, S., Ji, C., Chen, T., Luo, J., et al. (2015). Ultrahigh pyroelectric figures of merit associated with distinct bistable dielectric phase transition in a new molecular compound: Di-n-Butylammonium trifluoroacetate. *Adv. Mater.* 27 (32), 4795–4801. doi:10.1002/adma.201501923
- Tang, Y., Sun, Z., Ji, C., Li, L., Zhang, S., Chen, T., et al. (2015). Hydrogen-Bonded displacive-type ferroelastic phase transition in a new entangled supramolecular compound. *Cryst. Growth Des.* 15 (1), 457–464. doi:10.1021/cg501529f
- Tang, Y.-Z., Yu, Y.-M., Xiong, J.-B., Tan, Y.-H., and Wen, H.-R. (2015). Unusual high-temperature reversible phase-transition behavior, structures, and dielectric-ferroelectric properties of two new crown ether clathrates. *J. Am. Chem. Soc.* 137 (41), 13345–13351. doi:10.1021/jacs.5b08061
- Wang, C.-F., Li, H., Li, M.-G., Cui, Y., Son, X., Wang, Q.-W., et al. (2021). Centimeter-sized single crystals of two-dimensional hybrid iodide double perovskite (4, 4-difluoropiperidinium) $_4\text{AgBiI}_8$  for high-temperature ferroelectricity and efficient X-ray detection. *Adv. Funct. Mater.* 31 (13), 2009457. doi:10.1002/adfm.202009457
- Xu, W.-J., Du, Z.-Y., Zhang, W.-X., and Chen, X.-M. (2016). Structural phase transitions in perovskite compounds based on diatomic or multiautomic bridges. *CrystEngComm* 18 (41), 7915–7928. doi:10.1039/c6ce01485b
- Xu, L., Mu, X., Chen, X.-G., Zhang, H.-Y., and Xiong, R.-G. (2021). Organic enantiomeric ferroelectrics with high piezoelectric performance: Imidazolium L- and D-camphorsulfonate. *Chem. Mater.* 33 (14), 5769–5779. doi:10.1021/acs.chemmater.1c01663
- Xu, Q., Ye, L., Liao, R. M., An, Z., Wang, C. F., Miao, L. P., et al. (2022). H/F substitution induced Large increase of  $T_c$  in a 3D hybrid rare-earth double perovskite multifunctional compound. *Chemistry* 28 (14), e202103913. doi:10.1002/chem.202103913
- Xue, J. P., Noh, H. M., Choi, B. C., Park, S. H., Kim, J. H., Jeong, J. H., et al. (2020). Dual-functional of non-contact thermometry and field emission displays via efficient  $\text{Bi}^{3+} > \text{Eu}^{3+}$  energy transfer in emitting-color tunable  $\text{GdNbO}_4$  phosphors. *Chem. Eng. J.* 382, 122861. doi:10.1016/j.cej.2019.122861
- Yang, C. K., Chen, W. N., Ding, Y. T., Wang, J., Rao, Y., Liao, W. Q., et al. (2019). The first 2D homochiral lead iodide perovskite ferroelectrics: [R- and S-1-(4-Chlorophenyl)ethylammonium] $_2\text{PbI}_4$ . *Adv. Mater.* 31 (16), e1808088. doi:10.1002/adma.201808088
- Ye, H. Y., Ge, J. Z., Tang, Y. Y., Li, P. F., Zhang, Y., You, Y. M., et al. (2016). Molecular ferroelectric with most equivalent polarization directions induced by the plastic phase transition. *J. Am. Chem. Soc.* 138 (40), 13175–13178. doi:10.1021/jacs.6b08817
- Zhang, L., Lu, Z., Han, P., Wang, L., and Zhang, Q. (2013). Synthesis and photoluminescence of  $\text{Eu}^{3+}$ -activated double perovskite  $\text{NaGdMg}(\text{W}, \text{Mo})\text{O}_6$  - A potential red phosphor for solid state lighting. *J. Mater. Chem. C* 1 (1), 54–57. doi:10.1039/c2tc00189f
- Zhang, H.-Y., Zhang, Z.-X., Song, X.-J., Chen, X.-G., and Xiong, R.-G. (2020). Two-dimensional hybrid perovskite ferroelectric induced by perfluorinated substitution. *J. Am. Chem. Soc.* 142 (47), 20208–20215. doi:10.1021/jacs.0c10686
- Zhang, R., Wang, Z., Xu, X., Mao, X., Xiong, J., Yang, Y., et al. (2021). All-inorganic rare-earth halide double perovskite single crystals with highly efficient photoluminescence. *Adv. Opt. Mater.* 9, 2100689. doi:10.1002/adom.202100689
- Zhao, M.-M., Zhou, L., Shi, P.-P., Zheng, X., Chen, X.-G., Gao, J.-X., et al. (2019). 3D organic-inorganic perovskite ferroelastic materials with two ferroelastic phases:  $\text{Et}_3\text{P}(\text{CH}_2)_2\text{FMn}(\text{dca})_3$  and  $\text{Et}_3\text{P}(\text{CH}_2)_2\text{Cl Mn}(\text{dca})_3$ . *Chem. Eur. J.* 25 (25), 6447–6454. doi:10.1002/chem.201900771
- Zhou, F.-L., Song, S.-T., Lun, M.-M., Zhu, H.-N., Ding, K., Cheng, S.-N., et al. (2021). A hybrid multifunctional perovskite with dielectric phase transition and broadband red-light emission. *J. Mol. Struct.* 1239, 130468. doi:10.1016/j.molstruc.2021.130468